

FE Modeling of a Flatfoot Deformity for Improving Surgical Planning

Zhongkui Wang¹, Kan Imai², Masamitsu Kido², Kazuya Ikoma²,
and Shinichi Hirai¹

¹Department of Robotics, Ritsumeikan University, Kusatsu, Japan

²Department of Orthopaedics, Kyoto Prefectural University of Medicine, Kyoto, Japan

Abstract: This work presents a finite element (FE) model of a flatfoot deformity to study its biomechanics and improve the surgical plan for individual patients. Despite being a common foot deformity, the biomechanics of flatfoot is not fully understood. Regarding the optimal surgery, foot surgeons have different opinions for individual patients. Studies using cadaver feet are difficult to manage due to individual differences in foot geometry; therefore, these studies have made limited contributions to improving surgical planning. One option for solving this problem is to use a computer-based model. Due to the essence of continuum mechanics, the FE method has been used to model the human foot for various applications. In this work, the software package ABAQUS[®] was used to model and simulate flatfoot. The geometries of bones and soft tissue of a flatfoot were generated from CT images and imported into ABAQUS[®] as separate parts, which were then assembled and meshed with linear tetrahedral elements. Typical ligaments, tendons, and plantar fascia were modeled manually and the approximate positions of origin and insertion were referenced from an anatomy book together with the instruction of foot surgeons. The contact interactions among bones, soft tissue, and the ground were modeled using the penalty method with friction. A total of 17 bones, 62 ligaments, 9 tendons, 6 plantar fascia segments, and 1 encapsulated tissue part were modeled. Balanced standing simulations were performed, and the stress distributions were compared with experimental measurements to validate the model. The validated model will be used to study flatfoot biomechanics and investigate the optimal surgery for individual patients.

Keywords: Flatfoot Deformity, Surgical Simulation, Biomechanics, Elasticity, Hyperelasticity

1. Introduction

Flatfoot is a common foot deformity in which the arch of the foot collapses, with the entire sole of the foot coming into complete or near-complete contact with the ground. Most people with flatfeet experience no obvious differences compared to people with normal feet. No medical treatments are needed for them. In mild cases, orthoses such as an arch support can be used to lessen discomfort. In severe cases, which mostly happen in adult acquired flatfoot deformity (AAFD), surgery must be performed. According to different conditions, the appropriate surgeries include: (1) medializing calcaneal osteotomy (MCO), in which the back part of the calcaneus is cut and shifted internally, (2) lateral column lengthening (LCL), in which an open wedge osteotomy is

performed between the calcaneus and cuboid and this “lengthens” the foot and rotates the foot back to its correct position, (3) tendon and ligament procedures, in which certain tendons (*e.g.*, the posterior tibial tendon) or ligaments (*e.g.*, spring ligament or deltoid ligament) need to be repaired, and (4) double or triple arthrodesis, in which the fusion of two or more foot joints is performed. For an individual patient, the foot surgeons tend to have different opinions regarding the optimal surgery. Although agreement could be achieved on a certain surgery, finding the optimal surgical procedures or parameters (*e.g.*, the incision position in the case of MCO or the thickness of the wedge in the case of LCL) is still a challenging task faced by the surgeons. Unfortunately, the trial and error method is not feasible in medical cases.

To improve this situation and also study the flatfoot biomechanics, physical models, such as a cadaveric foot, have been used by researchers. Due to the lack of donors, healthy foot samples were often used to manually generate a flatfoot deformity by releasing or sectioning specific ligaments and tendons (Kitaoka, 1998; Niu, 2008). However, these artificially generated flatfoot samples do not fully reproduce the functions of a real flatfoot deformity. In addition, flatfoot patients usually have different foot deformities. Therefore, research results on artificial flatfoot samples do not provide much information to foot surgeons.

Computer-based models, meanwhile, can cope with the individual differences of flatfoot deformities and can easily simulate different surgical situations. The finite element (FE) method has been used frequently to model the human foot because of its essence of continuum mechanics and its capability of modeling irregular geometry and complex material properties. Cheung *et al.* presented an FE foot model to study the effects of soft tissue stiffening on stress distribution of the plantar surface during balanced standing (Cheung, 2005). The same model was also used to study the biomechanical effects of different types of foot orthosis for improving footwear design (Cheung, 2006). A foot-boot model was built for the future study of footwear design and parachute landing impact for the military (Qiu, 2011). FE foot models were also proposed for studying a clawed hallux deformity (Isvilanonda, 2012) and for developing an ankle prosthesis (Ozen, 2013), respectively. Unfortunately, only one FE model has been found to work for flatfoot, which was presented by Lewis in his PhD dissertation (Lewis, 2008). In his model, 14 bone segments, 65 ligaments, and a part of the plantar soft tissue were included, but the toes and dorsal soft tissue were missing. Regarding the development of FE models, commercial FE software packages are frequently used by researchers, such as ABAQUS[®] (Cheung, 2005; Cheung, 2006; Lewis, 2008; Ozen, 2013), ANSYS[®] (Qiu, 2011), and LS-DYNA[®] (Isvilanonda, 2012). In our previous work, we have developed a dynamic FE model of flatfoot without using commercial FE software. The model was used to simulate balanced standing, and simulated stress distribution was compared with measurements (Wang, 2014). Unfortunately, the contact and friction among neighboring bones were not formulated in the model, and neighboring bones were connected by soft tissue instead. This results in relatively stiff joints and further affects the model performance.

In this paper, the flatfoot was modeled using the commercial FE package ABAQUS[®]. The geometries of bones and tissue were generated from CT images. Ligaments, plantar fascia, and tendons were modeled manually as either 3D solid parts or tension-only wire parts. The approximate positions of origin and insertion of these tissues were referenced from an anatomy book together with the instruction of foot surgeons. Contact interactions were modeled with the penalty method. The tibia and fibula were fixed in space, and a ground plate was loaded and

pushed upward with half of the body weight to simulate a balanced standing situation. The simulation results with different material properties of encapsulated tissue and different boundary conditions of the ground plate were presented and compared with each other and also with experimental measurements.

2. Methods

2.1 Geometry Generation of Bones and Encapsulated Tissue

The flatfoot (right foot) geometries were generated from a series of CT images obtained from a male volunteer, 38 years old, 168 cm in height, and 62 kg in weight. During the CT scan, a custom-made foot loading device was used to fix the subject's lower limb (Kido, 2011). The boundaries of the bones and encapsulated tissue were segmented from CT images using Mimics[®] (Materialise Inc., Leuven, Belgium). The resulting boundary meshes were imported into a free mesh editor called Meshlab (<http://meshlab.sourceforge.net/>). The meshes were smoothed, and node densities were reduced to save computation time in the FE simulation. The simplified surface meshes (Fig. 1) were saved as ".stl" files. A free MATLAB[®] file converter called "CONVERT_stl_to_sat.m" was then used to convert the ".stl" files into ".sat" files, which can be imported into ABAQUS[®]. The bone structure consists of 17 segments: tibia, fibula, talus, calcaneus, cuboid, navicular, cuneiform (3 merged into 1), 5 metatarsals, and 5 phalanges (proximal, middle, and distal phalanges were merged together). These bone instances were cut out from the tissue instance to generate an encapsulated tissue instance surrounding the bones.

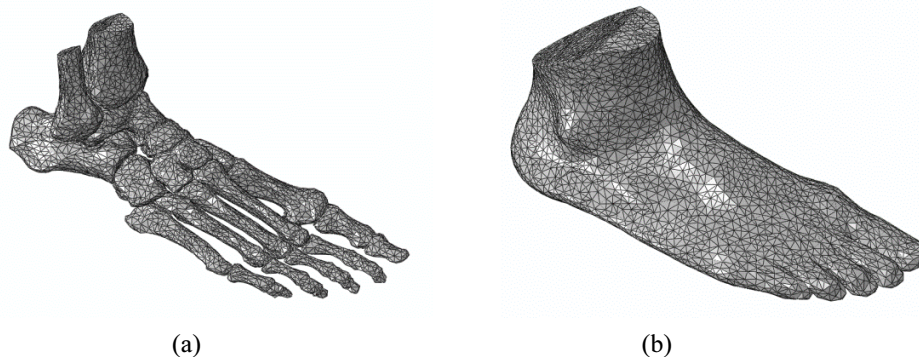


Figure 1. Surface geometrical meshes of (a) the bone structure and (b) the encapsulated soft tissue.

2.2 Geometry Generation of Ligaments, Plantar Fascia, and Tendons

To connect the bones to each other, and apply tendon forces to certain bones, the modeling of ligaments, plantar fascia, and tendons is necessary. However, from CT images, it is difficult to

discriminate ligaments, plantar fascia, and tendons from the surrounding tissue. To this end, the geometries of these tissues were generated manually by referring to an anatomy book (Netter, 2011) and also by following the suggestions of foot surgeons. Two different methods were used to model these tissues. One method models these tissues with simple wire parts (Fig. 2), and the second method uses 3D solid parts (Fig. 3). All of the foot models found in the literature use the first method, in which the end nodes of the wire parts were manually selected to approximately represent the origin and insertion positions of the ligaments and plantar fascia. The joint capsules connecting metatarsals and phalanges were modeled by four wire parts surrounding the two bones. Plantar fascia was divided into 6 separate wire parts connecting the calcaneus and the metatarsals, in which 2 wire parts were used to connect the calcaneus and two sesamoid bones on the 1st metatarsal bone. Tendons were not explicitly modeled in this method. Instead, tendon forces were applied directly on the appropriate nodes on corresponding bones. A total of 82 wire parts were generated in this model to represent the ligaments and plantar fascia.

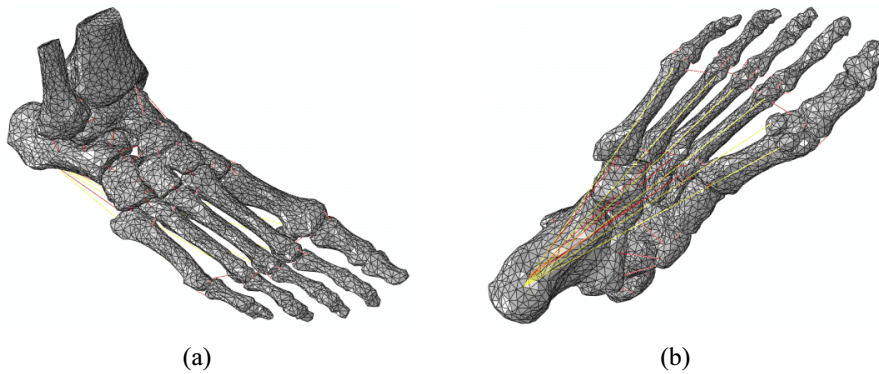


Figure 2. (a) Tarsal and (b) plantar views of the generated wire ligaments (red) and plantar fascia (yellow)

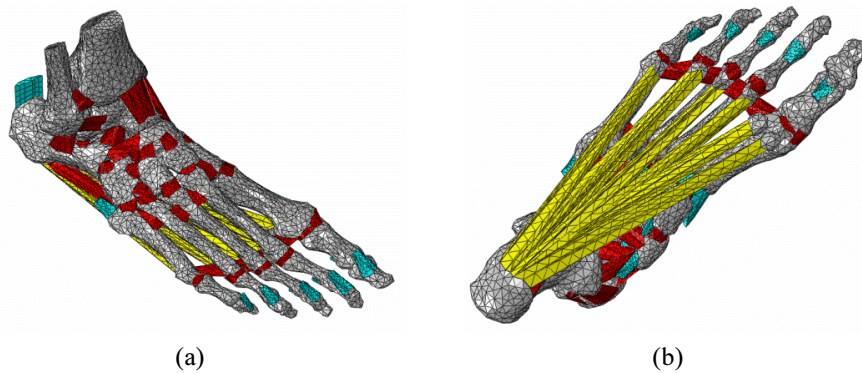


Figure 3. (a) Tarsal and (b) plantar views of the generated 3D solid ligaments (red), plantar fascia (yellow), and tendons (cyan).

The first method has the advantage of easy construction, but simplifying ligaments and plantar fascia into wires might lead to unrealistic results. Therefore, the second method was proposed, in which these tissues were constructed as 3D solid parts. First, several nodes were manually selected on the neighboring bones to approximate the origin and insertion positions of the ligament or fascia. The selected nodes were then connected with each other to construct a 3D surface mesh to form the ligament (red in Fig. 2) or plantar fascia (yellow in Fig. 2). Tendons (cyan in Fig. 2) were modeled in the same way, and the insertion end was represented by several nodes selected from the corresponding bone surface. The other end, which represents the cut position of the tendon, was manually constructed using a surface with the normal direction aligning with the loading direction of the tendon force. The joint capsules were also divided into 4 solid parts, and they could cover almost 360 degrees around the joint. The plantar fascia was also divided into 6 parts, and these parts could cover a large area on the foot bottom. Modeling with 3D solid parts gives us a more realistic representation of the ligaments, plantar fascia, and tendons, but the modeling process is more complicated than using wire parts. The performance of both methods will be demonstrated in this paper. In addition, to simulate balanced standing, a horizontal ground plate was created directly under the flatfoot model to support it.

2.3 Meshing the Parts

All of the solid parts, except the ground plate, were modeled with a 4-node linear tetrahedron “C3D4” element, and the wire parts were modeled with a 2-node linear truss “T3D2” element. The ground plate was modeled with an 8-node linear brick “C3D8R” element. The total number of nodes for the first and second models is 33,259 and 40,011, respectively. The total number of elements for both models is 131,309 and 148,108, respectively.

2.4 Material Properties

All of the materials were considered isotropic and linearly elastic except for the encapsulated tissue, which was modeled with both linear elastic material and nonlinear elastic material (hyperelastic) properties. Linearly elastic properties were listed in Table 1, and the hyperelastic properties (the second order polynomial model) of the encapsulated tissue were listed in Table 2, where the referenced literature was also indicated.

Table 1. Linearly elastic material properties

Component	Young's Modulus E (MPa)	Poisson's Ratio ν
Bone	7,300 (Cheung, 2006, Qiu, 2011)	0.3 (Cheung, 2006, Qiu, 2011)
Ligament	260 (Cheung, 2006, Qiu, 2011)	0.4 (Cheung, 2006, Qiu, 2011)
Plantar Fascia	350 (Cheung, 2006, Qiu, 2011)	0.4 (Cheung, 2006, Qiu, 2011)
Tendon	1,500 (Peltonen, 2010)	0.4 (Peltonen, 2010)
Encapsulated Tissue	2.49 (Isvilanonda, 2012)	0.49 (Isvilanonda, 2012)
Ground	17,000 (Cheung, 2006, Qiu, 2011)	0.1 (Cheung, 2006, Qiu, 2011)

Table 2. Hyperelastic properties (nonlinear material)

C_{10} (MPa)	C_{01} (MPa)	C_{20} (MPa)	C_{11} (MPa)	C_{02} (MPa)	D_1 (MPa ⁻¹)	D_2 (MPa ⁻¹)
0.08556	-0.05841	0.03900	-0.02319	0.00851	3.65273	0.00000

The data were referenced from the literature (Cheung, 2005; Cheung, 2006; Qiu, 2011).

2.5 Contact Interactions and Constraints

Contact interactions among neighboring bones and between the encapsulated tissue and the ground plate were modeled using penalty tangential behavior with a friction coefficient of 0.6 and the discretization method is defined as “surface to surface”. A total of 21 contact pairs were defined. Tie constraints were created to connect ligaments and plantar fascia to corresponding bones and also to connect bones and the encapsulated tissue. A total of 183 tie constraints were defined in the models.

2.6 Loading and Boundary Conditions

As shown in Fig. 4, to simulate balanced standing, the top surfaces of the tibia, fibula, and encapsulated tissue were fixed in space. The ground reaction force and the Achilles tendon force were applied in the model. The ground reaction force was applied as the pressure load with half of the body weight (32 kg) acting on the ground surface underneath. Only the Achilles tendon force was considered, and the forces on the other tendons were neglected (Cheung, 2006). The Achilles force was assumed to be 50% of the ground reaction force (Lewis, 2008) which is half of the body weight. Therefore, the Achilles force is calculated as 25% of the body weight, which is 151.9 N. Both loads were applied as a ramp function of time.

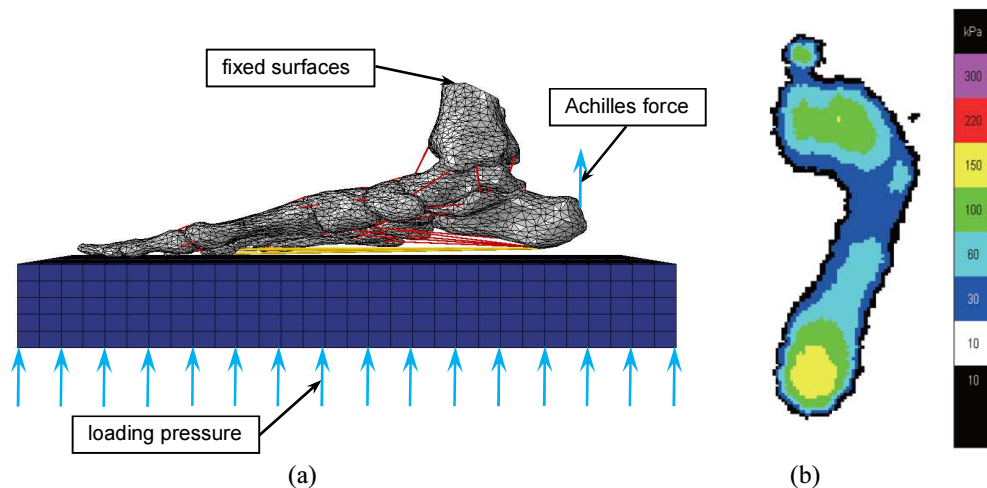


Figure 4. (a) Loading and boundary conditions defined in the model and (b) measured plantar stress distribution.

2.7 The Measurement of Plantar Stress during Balanced Standing

To validate the FE model, experiments of balanced standing were performed with the same subject for the CT scan. The measurements were obtained using an Emed-M[®] pressure platform system.

Three measurements were taken on both feet, and the average stress of the right foot was calculated (Fig. 4b) and compared with the simulation results.

2.8 Sensitivity Studies of Linear Material Property and Boundary Condition

The material properties of the encapsulated tissue significantly affects the stress distribution. Therefore, sensitivity analysis was conducted to evaluate the sensitivity of the Young's Modulus of the encapsulated tissue. Different Young's Moduli, as shown in Table 3, were evaluated, in which $E1 = 2.49$ MPa is used from the literature (Isvilanonda, 2012), and $E2$, $E3$, $E4$ were selected as $1/2$, $1/5$, and $1/10$ of $E1$. The reason why we only focus on the values smaller than the original value ($E1$) is because we found that $E1$ is a very large value and deformation on the foot bottom is very small during balance standing. The deformation results will be shown in the next section.

In the initial state of the model, the flatfoot bottom is parallel to the surface of the ground plate and the loading direction of the ground plate is perpendicular to this surface. However, this loading direction may change during the simulation of balanced standing, similar to the way human beings may adjust their longitudinal axis to achieve a stable standing position. Therefore, in the simulation, three different boundary conditions of the ground plate, as shown in Table 4, were simulated to evaluate the differences. In the first case (BC 1), the ground plate was loaded along the longitudinal axis (z -axis) and no other motions were allowed. In the second case (BC 2), the ground plate was loaded longitudinally while it was also allowed to rotate around the coronal axis (x -axis). In the third case (BC 3), the ground plate was allowed to move in all 6 degrees of freedom.

Table 3. Different Young's Modulus of the encapsulated tissue

Case	E1	E2	E3	E4
Young's Modulus E (MPa)	2.49	1.245	0.498	0.249

Table 4. Different boundary conditions of the ground plate

Case	BC 1	BC 2	BC 3
Boundary Conditions	U1=0, U2=0, U3=Free, UR1=0, UR2=0, UR3=0	U1=0, U2=Free, U3=Free, UR1=Free, UR2=0, UR3=0	U1=Free, U2=Free, U3=Free, UR1=Free, UR2=Free, UR3=Free

U1, U2, and U3 indicate translation motion along the x -, y -, and z -axis. UR1, UR2, and UR3 indicate the rotation around the x -, y -, and z -axis. The x -, y -, and z -axis are aligned with the coronal, the sagittal, and the longitudinal axis, respectively.

2.9 Solver Information and Performance Metrics

Three steps were defined in Abaqus/Standard for the balanced standing simulation. They are: initial, contact (1sec), and load (1sec) steps. For simulations with nonlinear properties of soft tissue, geometric nonlinearity flag "NLgeom" was turned on, but not for simulations with linear properties. The total number of the variables in the model is 127380. The total CPU time is 2516.8sec and 2848.4sec, respectively, for models with linear and nonlinear properties of the encapsulated tissue.

3. Results and Discussion

The simulation results of plantar stress in different models were shown in Fig. 5. We found that modeling the ligaments and plantar fascia with either wire or solid parts does not yield an appreciable difference in the stress distribution. This finding gives us more confidence in using the wire parts to model these tissues because the construction of the wire parts is less time-consuming. Comparing the results between the linear and nonlinear models, we found that the stress was distributed more evenly in the nonlinear model but was more concentrated in the middle and rear of the foot in the linear model. We also found that the linear elastic material is much harder than the nonlinear hyperelastic material. The maximal displacements of the reference node on the different models are: 0.1525 mm in Fig. 5a, 0.1339 mm in Fig. 5b, and 1.3422 mm in Fig. 5c. The

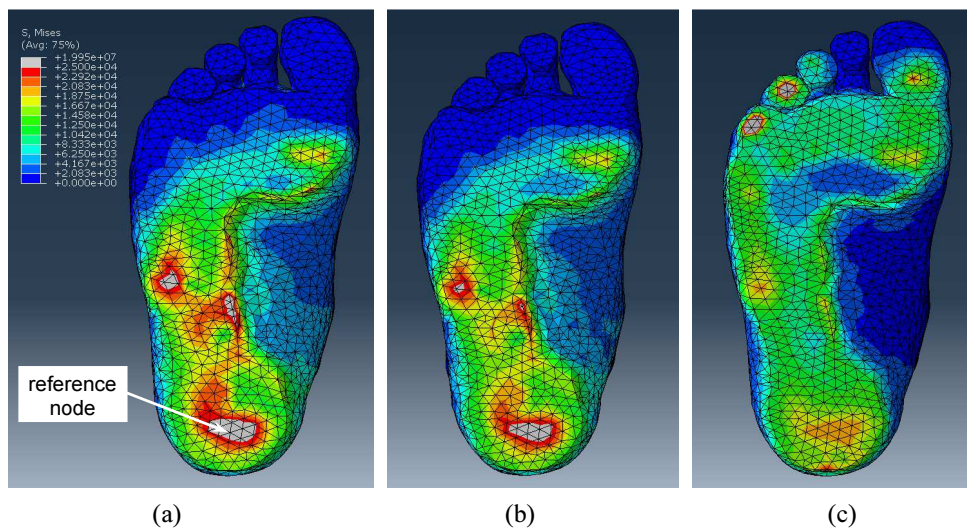


Figure 5. The simulation results of plantar stress from different models: (a) linear elastic tissue with wire ligaments and plantar fascia, (b) linear elastic tissue with 3D solid ligaments and plantar fascia, and (c) nonlinear hyperelastic tissue with 3D solid ligaments and plantar fascia.

displacement is almost 10 times larger in the nonlinear model compared with the linear model. The results of the parametrical studies will be discussed later in the paper. Furthermore, we found that the simulation results (Fig. 5) were not consistent with the experimental measurements (Fig. 4b). In our experiments, plantar stress was distributed mostly in the forefoot and heel areas, and some stress also appeared in the big-toe area. However, in the simulation results with linear models, higher plantar stress was distributed mostly in the middle and heel areas, and slightly in the forefoot area under the sesamoid bones. Two reasons may cause these differences. One is the geometry of the mesh. To obtain a relatively stable initial state, the CT images were taken while the subject was lying on the CT table with his lower limb fixed by a custom-made device. While

the measurements were taken, both feet were subjected to $5.7 \pm 2.6\%$ of the subject's body weight (Kido, 2011). This initial loading makes the initial geometry of the plantar surface relatively flat, rather than its natural curved surface in which the forefoot and heel areas usually have a lower profile compared with the middle foot area. This fact explains why a greater amount of stress occurs at the forefoot area in the experiments but the middle foot area in simulation. Another reason concerns the stress on the big toe. Stress on big toe appears in the experiment but not in the simulation (linear model). This finding may be caused by the ground loading direction or the ground boundary condition, which will be discussed later. If we compare Fig. 5c to Fig. 4b, we found that the nonlinear model results in some stress on the big toe as observed in the experiment, but there was also very high stress at the fourth and fifth toes, which is not a normal occurrence. This observation was also caused by the initial mesh. There are very thin tissue layers in between the phalange distal bones and the ground plate, especially in the fourth and fifth toe areas. When these thin layers are in contact with the ground plate, the stress increases more quickly than in other parts of the tissue. Figure 6 shows a comparison of simulated plantar stress using different material properties of the encapsulated tissue and with different boundary conditions of the ground plate. We found that if the encapsulated tissue became softer, the plantar stress would distribute more evenly, the contact area would slightly increase, and the maximum stress would decrease for all three cases of boundary conditions. The maximal displacements of the reference node in the boundary condition BC 1 are 0.1525 mm, 0.2574 mm, 0.5249 mm, and 0.8848 mm along with a decrease of Young's Modulus. Even the softest tissue yielded a smaller displacement than the model with nonlinear hyperelastic tissue. Therefore, we believe that the original linear elasticity of 2.49 MPa for the encapsulated tissue is a relatively large and inappropriate value. From Fig. 6, we also found that the boundary condition of the ground plate affects the plantar stress distribution. Allowing for the rotation motion of the ground plate shifts the plantar stress towards the forefoot and distal areas and a greater consistency with the experimental measurements. With a softer encapsulated tissue, boundary condition case 2 and case 3 do not result in an appreciable difference in plantar stress.

Figure 7 shows the simulated plantar stress with different boundary conditions for the model with a hyperelastic encapsulated tissue. We again found that the rotation of the ground plate affects the plantar stress, and the boundary condition BC 3 shows the best performance. If we compare Fig. 7 with Fig. 6, we found that the nonlinear model yields better results compared with the linear model. In addition, we found that the peak stress in our simulations is quite small compared with the experimental measurements and published data. Peak stresses in our simulations are 28.34 KPa, 27.85 KPa, and 20.22 KPa for the results shown in Fig. 5a, 5b, and 5c, respectively. However, the peak stress in the experimental measurements is 165 KPa. Published data on simulated peak stress in a healthy foot were found to be 131 KPa (Antunes, 2010), 168 KPa (Chen, 2001), 198 KPa (Qiu, 2011), and 230 KPa (Cheung, 2005), respectively. We believe that this difference is also caused by the initial mesh geometry of the flat plantar surface, which increases the contact area of the foot when it comes in contact with the ground. As a result, the stress amplitude on the plantar surface and the peak stress are decreased. This discrepancy could be improved by using foot geometry with a natural curved plantar surface. However, it is difficult to ensure the stability of the foot during a CT scan. Such stability will be one of our future tasks.

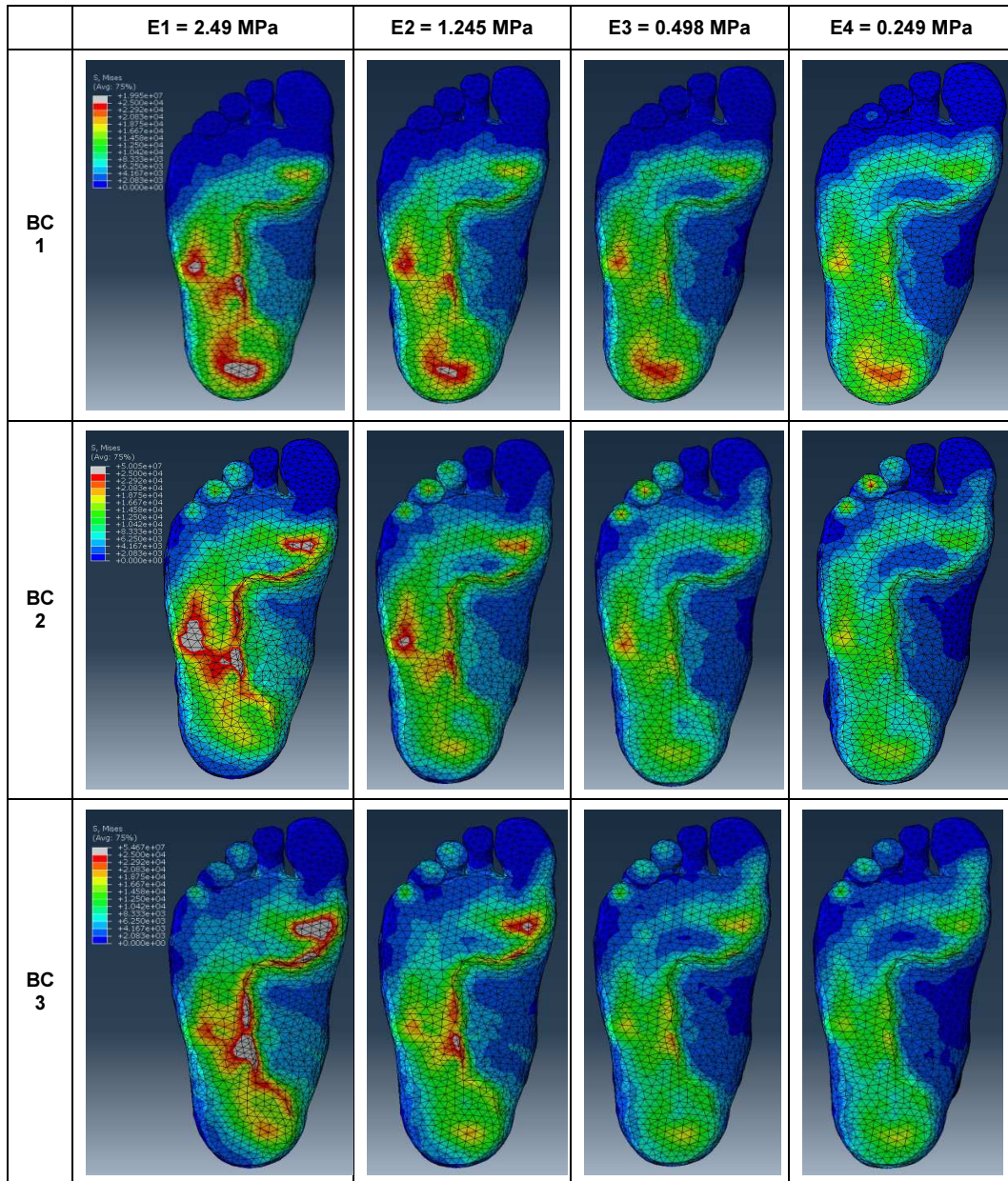


Figure 6. Simulated plantar stress distribution with different material properties (E) of encapsulated tissue and different boundary conditions (BC) of the ground plate.

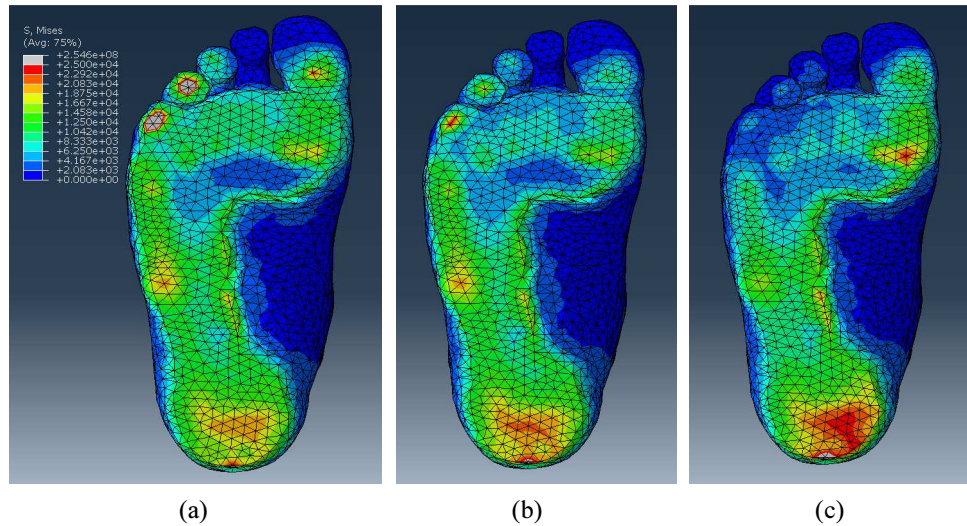


Figure 7. Simulated plantar stress with different boundary conditions: (a) BC 1, (b) BC 2, and (c) BC 3 for the model with nonlinear hyperelastic tissue.

4. Conclusion

To better study flatfoot biomechanics and improve the decision-making for flatfoot surgery, a computer model of flatfoot with detailed anatomical structures is one of the options. In this study, a 3D FE model of a flatfoot was developed using the 3D reconstruction of CT images. Two methods for manually modeling ligaments, plantar fascia, and tendons were introduced. Balanced standing simulations were performed using different tissue properties and different boundary conditions. The simulation results of plantar stresses were compared with experimental measurements to validate the proposed models. Through the comparisons, three conclusions were made. First, modeling ligaments and plantar fascia with wire parts (truss element) has almost the same performance compared with 3D solid parts. Therefore, modeling with wire parts will be used in our future work because it is less time-consuming for model construction. Second, the material properties of the encapsulated tissue and the boundary condition of the ground plate affect the plantar stress distribution. The boundary condition BC 3 yields the best performance in both the linear and nonlinear models. Compared with the linear model, results of the nonlinear model are more consistent with the experimental measurements. Therefore, the nonlinear model will be used in our future work. Third, simulation results using current geometry with a flat plantar surface are not consistent with the experimental measurements. A relatively curved plantar surface will improve the consistency to some extent and will be investigated in our future work. Modeling and simulation of a healthy foot will also be conducted to compare the difference with a flatfoot. After validating our flatfoot model, surgical simulation, such as MCO and LCL, will be performed and

we hope that these simulations will contribute to the development of an optimal surgery plan and a tailor-made surgery for individual patients.

5. References

1. Antunes, P. J., Dias, G. R., Coelho, A. T., Rebelo, F., Pereira, T., “Non-Linear Finite Element Modeling of Anatomically Detailed 3D Foot Model,” Online Available.
2. Chen, W., Tang, F., and Ju, C., “Stress Distribution of the Foot during Mid-stance to Push-Off in Barefoot Gait: A 3-D Finite Element Analysis,” *Clinical Biomechanics*, vol. 16, no. 7, pp. 614-620, 2001.
3. Cheung, J. T. M., Zhang, M., Leung, A. K. L., and Fan, Y., “Three-Dimensional Finite Element Analysis of the Foot During Standing-A Material Sensitivity Study,” *Journal of Biomechanics*, vol. 38, no. 5, pp. 1045-1054, May, 2005.
4. Cheung, J. T. M., Zhang, M., “Finite Element Modeling of the Human Foot and Footwear,” *ABAQUS Users’ Conference*, pp. 145-159, 2006.
5. Isvilanonda, V., Dengler, E., Iaquinto, M., Sangeorzan, B. J., and Ledoux, W. R., “Finite Element Analysis of the Foot: Model Validation and Comparison between Two Common Treatments, of the Clawed Hallux Deformity,” *Clinical Biomechanics*, vol. 27, no. 8, pp. 837-844, 2012.
6. Kido, M., Ikoma, K., Imai, K., Maki, M., Takatori, R., Tokunaga, D., Inoue, N., and Kubo, T., “Load Response of the Tarsal Bones in Patients with Flatfoot Deformity: In Vivo 3D Study,” *Foot Ankle Int.*, vol. 32, no. 11, pp. 1017-1022, Nov., 2011.
7. Kitaoka, H. B., Luo, Z., and An, K., “Three-Dimensional Analysis of Flatfoot Deformity: Cadaver Study,” *Foot & Ankle International*, vol. 19, no. 7, pp. 447-451, 1998.
8. Lewis, G. S., “Computational Modeling of the Mechanics of Flatfoot Deformity and Its Surgical Corrections,” Ph.D. Dissertation, Pennsylvania State University, 2008.
9. Netter, F. H., “Atlas of Human Anatomy,” Fifth Edition, Elsevier, pp. 51-525, 2011.
10. Niu, W., Yang, Y., Fan, Y., Ding, Z., and Yu, G., “Experimental Modeling and Biomechanical Measurement of Flatfoot Deformity” in *Proc. 7th Asian-Pacific Conference on Medical and Biological Engineering (IFMBE)*, vol. 19, pp. 133-138, 2008.
11. Ozen, M., Sayman, O., and Havitcioglu, H., “Modeling and Stress Analyses of A Normal Foot-Ankle and A Prosthetic Foot-Ankle Complex,” *Acta of Bioengineering and Biomechanics*, vol. 15, no. 3, pp. 19-27, 2013.
12. Peltonen, J., Cronin, N. J., Avela, J., and Finni, T., “In Vivo Mechanical Response of Human Achilles Tendon to A Single Bout of Hopping Exercise,” *The Journal of Experimental Biology*, vol. 213, pp. 1259-1265, 2010.
13. Qiu, T., Teo, E., Yan, Y., and Lei, W., “Finite Element Modeling of a 3D Coupled Foot-Boot Model,” *Medical Engineering & Physics*, vol. 33, no. 10, pp. 1228-1233, Dec., 2011.
14. Wang, Z., Imai, K., Kido, M., Ikoma, K., and Hirai, S., “A Finite Element Model of Flatfoot (Pes Planus) for Improving Surgical Plan,” *Proc. In 36th Annual International Conference of the IEEE Engineering in Medicine & Biology Society*, pp. 844-847, Chicago, Aug., 2014.